# CHALMERS

Near-Infrared Transillumination of Dental Tissues
Methods for image processing and assisted diagnosis

Master of Science Thesis in Biomedical Engineering, MPBME

GUSTAV HENMAN

Clarification

This thesis is written as a part of a double master's degree exchange between Chalmers University of Technology (CTH) in Göteborg and Bauman Moscow State Technical University (BMSTU). The thesis work has been carried out at BMSTU but will be defended at both Universities. Supervisor at BMSTU is Professor Igor Nikolaevich Spiridonov. Examiner at CTH is Professor Yngve Hamnerius.

Abstract

A system currently developed at Bauman Moscow State Technical University based on a patented method for image capturing through near-infrared transillumination (NIRTI), can provide a non-ionizing, real-time method for dental imaging. This could both eliminate the patient ionizing radiation exposure and possibly increase the quality of dental diagnostics. Except for providing a possibility to detect early caries lesions, the method also enables imaging of blood vessels. This opens up a new field of dental diagnostics focusing on detection and analysis of vascular structures. There is a number of diseases which affect the dimensional and structural properties of the gingival blood vessels, for example gingivitis and periodontitis. Blood vessel properties could also be used to calculate vascular density which could give a hint of tissue oxygenation, a very diagnostically interesting parameter. The main goal is to develop methods for blood vessel imaging to automatically quantify vascular structures.

The developed image processing methods consist of contrast enhancement followed by local thresholding for segmentation and detection of the blood vessels. A comparison between the mask of the detected blood vessels and the reference mask shows that 67 % of the vascular tissue and 93 % of the non vascular tissue is detected correctly. The reason for the low vascular classification rate is mainly due to light artifacts.

An algorithm to extract structural parameters like length and diameter and topological parameters like hierarchal order has also been developed. To test the parameter extraction algorithm, it has been applied to the vascular mask of an image captured by the NIRTI prototype. The algorithm output consists of extracted parameters for each segment of the structure, the total value of each parameter (total blood vessel length, total area etc.) and finally a value of vascular density.

In order to develop a NIRTI system able to perform both caries detection and vascular imaging, the system needs to be equipped with at least two different modes, one for each purpose. Further development of methods for assisted diagnosis should advantageously be performed in close cooperation with dentists to identify the most valuable information to acquire and present. Another part of future research involves optimizing the image processing algorithms for real time processing, which of course is a prerequisite for real time diagnosis.

Abbreviations

BMSTU = Bauman Moscow State Technical University

CCD = Charged-Coupled Device

CMOS = Complementary Metal–Oxide–Semiconductor

CTH = Chalmers University of Technology

InGaAs = Indium Gallium Arsenide

IR = Infrared

NIR = Near-Infrared

NIRTI = Near-Infrared Transillumination

OCT = Optical Coherence Tomography

TI = Transillumination

Contents

1. Introduction

This master thesis concerns study and development of image processing methods for Near-Infrared Transillumination (NIRTI) in dental applications. The first chapter gives an introduction to the topic and a summary of the main questions.

1.1 Previous research at BMSTU

The work on dental NIRTI is a part of research carried out at Bauman Moscow State Technical University (BMSTU) within development of a new imaging system for stomatology (Spiridonov, 1996). Today's diagnostics in stomatology have a couple of shortcomings:

- most dental diagnostics is performed with dental radiographs (x-ray) with ionizing influence on tissues
- when performing real time diagnosis with x-ray, the ionizing radiation is an even bigger issue (Gottlow, 2012)
- diagnostic information provided by old instrumental methods are limited and could be extended by implementation of new methods and technology
- there is a lack of methods for quantitative description of dental diseases

A non-ionizing, real-time system for dental imaging could both eliminate the patient radiation exposure and possibly increase the quality of dental diagnostics. The system currently developed at BMSTU is based on a patented method (Spiridonov, et al., 1998) from 1998 for image capturing through NIRTI. By registering backscattered NIR light transilluminated through human tissue, an image with enough contrast between different tissues can be captured. In section 2.3, this method is explained in further detail. Except for providing a possibility to detect early caries lesions the method also enables imaging of blood vessels thanks to the deviant optical properties of blood. This opens up a new field of dental diagnostics focusing on detection and analysis of vascular structures.

A prototype of the equipment for NIRTI has previously been constructed at BMSTU (Figure 1). Images captured with this equipment have a limited image quality, resolution and contrast level. A new version of the system is under development and an important part of this research concerns methods for image processing, the topic of this thesis. Development of these image processing methods includes contrast enhancement for teeth and blood vessel

images, automated detection of blood vessels and quantification of vascular structures. The main objective with the study of vascular structures is to provide dimensional and structural information to assist in diagnosis.
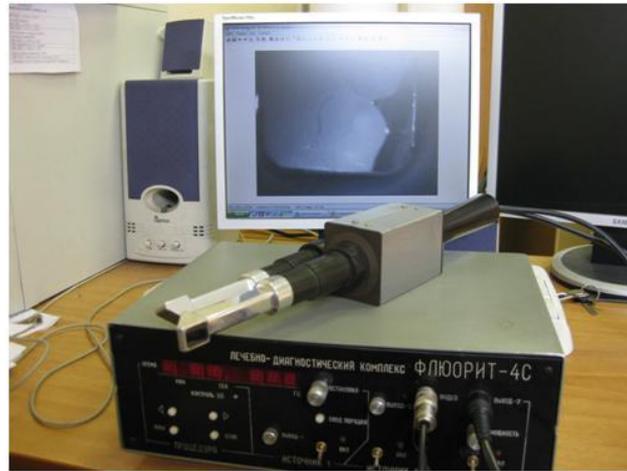
Figure 1. *Prototype of the NIRTI system.*

During the work with this thesis, a number of Russian journal and conference articles have been published. Consequently, most of the content in Chapter 5, Results, has previously been presented in forms of articles. With this said, no references to these publications have been made in the text, but a list of articles can be found in Appendix I.

1.2 Dental diagnostic applications

This is a brief view of diagnostic applications of NIRTI with the aim to anchor the research in medical demands. The applications in the dental field can be divided in the two parts, one concerning teeth and one focusing on gingival diagnostics.

1.2.1 Teeth diagnostics

The by far most investigated and developed application for NIRTI in dental diagnosing is caries detection. The optical properties of early lesion crystallizations make it possible to detect caries at an earlier stage than with traditional dental radiology (see section 2.3). The absence of ionizing radiation combined with convenient size of the equipment makes it possible to perform real-time diagnosis. This is also something that could be of great help when searching for other structural changes in teeth, which can be hard to detect with x-ray (Ekestubbe, 2012). Combined with image processing algorithms for detection of suspected caries lesions or other structural changes, NIRTI could become, if not a supplement at least a

powerful compliment to dental x-ray. In section 3.1, results from some of the previous studies carried out on NIRTI for caries detection are summarized.

Thanks to the simplicity and relatively low price of the NIRTI equipment, another interesting path could be to focus on the developing world where there are billions of people who do not have access to dental care (Dentists without borders, 2012). If a version is developed with relatively standardized components, connected with a standard PC, the overall cost of standardized dental care would decrease, and the competence requirements for using the equipment would be substantially lower than these for the X-ray.

1.2.2 Gingival diagnostics

A new and fairly unexplored field of use for NIRTI is in diagnosis of the gingiva. Interviews with both special and common care dentists suggest that the technology could be truly valuable for gingival use (Gottlow, 2012), (Ekestubbe, 2012). Since the near-infrared light gives a contrast between blood vessels and underlying tissue (see section 2.3) it can be used to image gingival blood vessels. There are a number of gingival related diseases which affect the dimensional and structural properties of the gingival blood vessels (Figure 2). The two most common and relevant states are gingivitis and periodontitis which both causes local inflammations and vascular expansion of the periodontium, i.e., the tissues that surround and support the teeth (Gottlow, 2012).
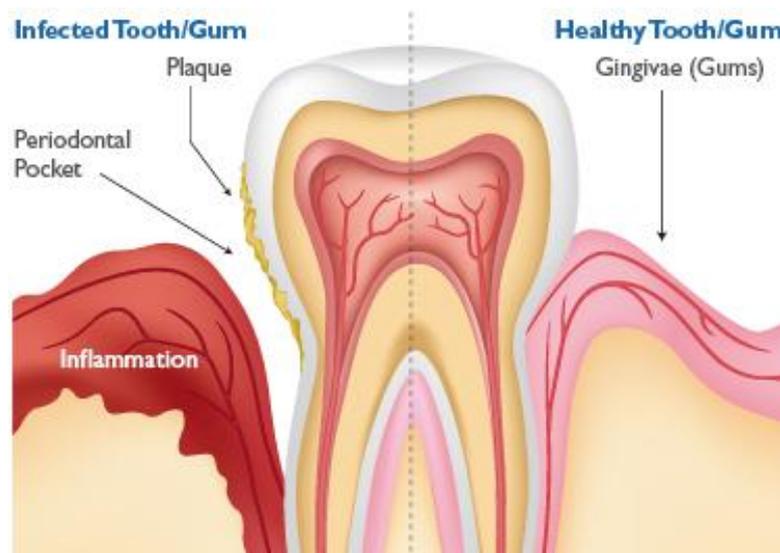

Figure 2. *Sign of periodontal disease* (**Anon., 2012**).

Another diagnostically valuable parameter is tissue oxygenation. One measure that could give a hint of a tissues oxygenation is the density of blood vessels in the present tissue, the vascular density (Shepro, 2006). With NIRTIs ability to detect blood vessels, this parameter could be calculated by the help of image processing algorithms. Measurement of vascular density can of course also be performed in other tissues of the body.

1.2.3 Other applications

Use of NIRTI based methods is of course not limited only to the oral cavity. During the research work, documentation and studies describing application of the imaging technique in others areas have been encountered. To mention some examples, NIRTI-based methods have been developed to assist in imaging of breast cancer, diagnosing maxillary sinusitis, visualize blood vessels to ease application of needles etc. For the complete list of alternative diagnostic applications of NIRTI see Appendix II.

1.3 Document overview

This thesis first gives an introduction to the NIRTI technology where the reader is provided with the necessary technical background. Then, a summary of some recent relevant research within the field of NIRTI is presented. Next chapter contains a problem statement which specifies the exact problems this thesis tackles. The research results are then presented divided into a smaller part concerning teeth images and a more extensive part regarding blood vessel imaging and quantification of vascular structures. Finally, conclusions are drawn on how well the result meets the problem statement. Reflections on the result and potential future research are also discussed here. Some figures, tables and other substantiated data have been consigned to the appendix.

2. A brief review of NIRTI

This section includes an introduction to infrared light and transillumination in general followed by a description of the particular NIRTI system developed at BMSTU.

2.1 Infrared light

Electromagnetic radiation with a wavelength longer than visible light, starting from 0.74 µm and reaching to 300 µm, is defined as infrared (IR) light. The first person ever observing IR light was the German astronomer William Herschel. In the year 1800 he made an important discovery by letting sunlight pass through a prism and then extending the conventional visible light spectrum with thermometers. He registered a higher temperature in the extension of the spectrum than at control points outside. In this way, Herschel showed that there are forms of light beyond the red light. Except for leading to the discovery of IR light, the experiment was the first to show that there are forms of light not visible for the human eye (Electrophysics, 2012).

The wavelength range of IR light corresponds to a frequency of about 1-400 THz, which for instance includes the majority of the thermal radiation emitted by objects in room temperature. On a microscopic level, IR light is emitted or absorbed by changes in the rotational-vibrational movements of molecules (Hewitt, 1993).

2.1.1 IR-band subdivisions

For convenience, since the capture capacities of IR sensors usually are limited to a certain bandwidth, the wavelengths included in the IR-band are divided into subsections. The near-infrared (NIR) region represents the lowest IR wavelengths reaching from 750 to 1400 nm and is defined by its water absorption capability. This is one of the properties that makes it suitable for medical transillumination purposes. Other examples of use for NIR light are in optic telecommunication due to its low attenuation losses and in night vision devices cause of image intensifiers sensitivity to NIR light. When moving higher in the IR spectrum applications like heat seeking sensors in homing missiles, thermal imaging and terahertz spectroscopy can be found (Byrnes, 2009). For a full description of all types of IR light, see Appendix III.

2.1.2 Health hazards

Cause of the limited penetration dept of IR radiation in biological tissue, the main health hazards are connected to skin and eyes. Most of the radiation's interaction with biological tissue is thermal. Depending on the IR wavelength (higher risk with longer wavelengths), high exposure of IR radiation to the skin can lead to local thermal effects or even burns in serious cases. However, the short wavelength and power of the radiation used in NIRTI does not constitute any danger.

The eye has a natural protection from optical radiation from the natural environment, but exposure from high concentration radiation from a laser or other point source can cause damage to the retina. Since the near-infrared IR light associated with NIRTI is included in this category, looking straight into the light source should be avoided (Matthes, 2010).

2.2 Transillumination

The technique of illuminating a sample by transmission of light is referred to as transillumination (TI). In the field of medicine this means transmission of light through parts of the body for imaging purposes. One of the first documented experiments of medical TI was performed by the Englishman R. Bright in London 1831 (Schmidt, 1999). He showed that light from a candle or sunlight could be used to shine through a head of a patient and make the cranium semi-transparent, which could help detection of brain tumors. Transillumination of tissue was noticed in 1843 by the surgeon T.B. Curling who used it to detect build-up of clear fluid in the testis. However, the real medical breakthrough came much later when M. Cutler used TI for monitoring of breast lesions (Tuchin, 2002). With this method he was able to differentiate normal and pathological tissue by observing shadows made by features beneath the surface.

In 1933 Pearson and Norris showed that near-infrared (NIR) light could be used for TI to further improve the contrast (Schmidt, 1999). However, because of autofluorescence and strong light scattering, these early studies of NIR only showed some general optical properties of tissue. In the coming decades many important studies related to TI were made, including research on the optical properties of hemoglobin, measurements on earlobes and cheeks showing the tissue spectra at the water band (980 nm) and deep TI of mammalian tissue. This was followed by the development of new time- and spatially resolved methods combined with the CCD-matrix for image capturing, which in turn led to the investigations of NIR for use in

other biomedical applications (Tuchin, 2002). This has led to a number of commercially available clinical monitoring and imaging instruments for NIR transillumination and spectroscopy.

2.3 Image formation and optics

The particular NIRTI system developed at BMSTU is based on a patent from 1998 by Professor I.N. Spiridonov et al. (Spiridonov, et al., 1998). What mostly differentiates this system from other NIRTI based solutions is the use of the wavelength 870 nm, which is shorter than the conventional. This enables the use of cheaper and simpler diodes instead of InGaAS technology, at the expense of lower contrast. A first prototype of the system, able to capture, process and store NIRTI images has been constructed. The following part of this section is all parts of previous research. A block diagram of the system layout is shown in Figure 3.
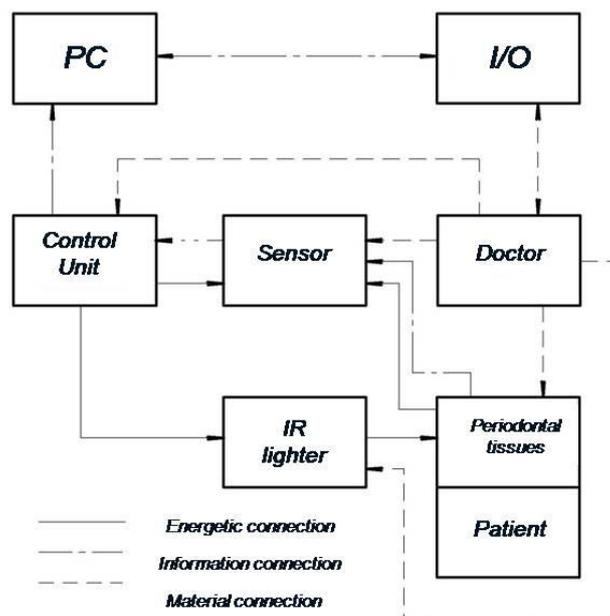

Figure 3. *Block diagram of the NIRTI system.*

A doctor locates the sensor and the laser IR lighter in the oral cavity of the patient and controls the intensity of the laser radiation by a control unit. A microvascular IR image is formed by backscattered radiation registered by a sensor (CCD matrix) and transmitted by a connecting interface to the PC for processing, storage and display.

Figure 4 describes the phenomenological model of interaction between infrared radiation and dental tissues.
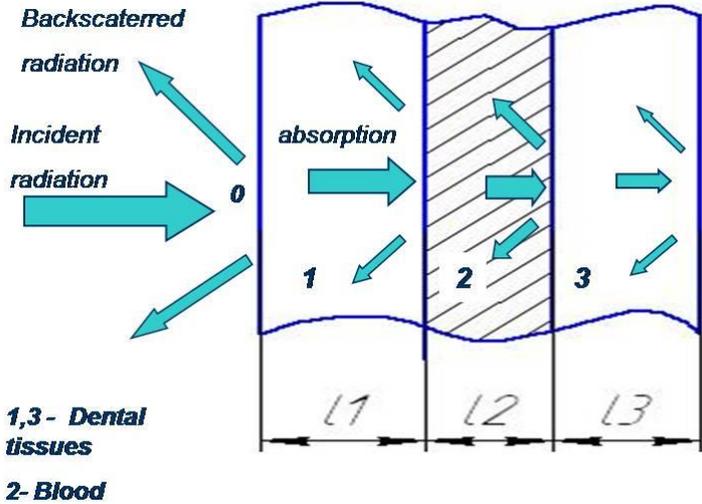
Figure 4. *Interaction between infrared radiation and dental tissue.*

The contrast between blood vessels and surrounding tissue is calculated with (1), where $n_k(\lambda)$ is the quantity of photons backscattered by tissue and $n_v(\lambda)$ is the quantity of photons backscattered by blood vessels (Belikov, et al., 2008).

$$C(\lambda) = \frac{n_h(\lambda) - n_v(\lambda)}{n_h(\lambda) + n_v(\lambda)} \tag{1}$$

Calculations show that the probe wavelength has to meet two demands. Figure 5 indicates that contrast between blood vessels and surrounding tissue increases with probe wavelength. The sensitivity of the CCD/CMOS sensors decreases with increased probe wavelength, illustrated in Figure 6.
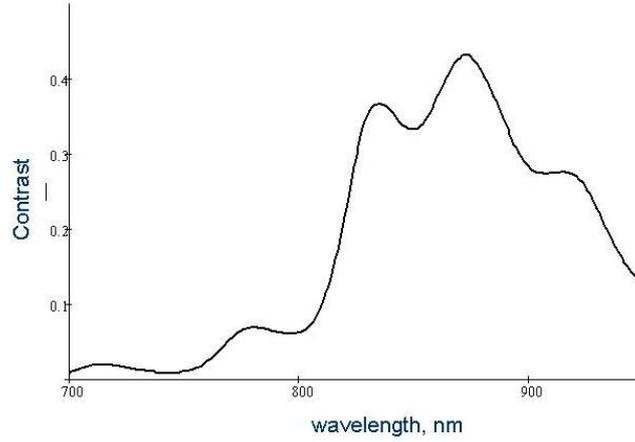
Figure 5. *Blood vessel contrast against probe wavelength.*
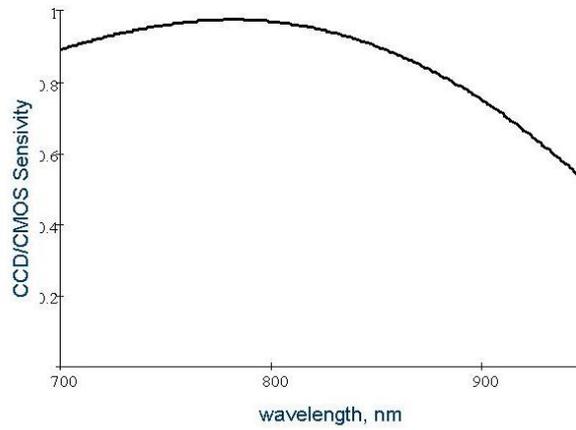
Figure 6. *CCD/CMOS-sensitivity against probe wavelength.*

The optimal value of the probe wavelength can be obtained by finding the minimum of,

$$\Phi(\lambda) = \frac{[C(\lambda) - C(\lambda_{max})]^2}{C(\lambda)^2}\alpha_1 + \frac{[S(\lambda) - S(\lambda_{min})]^2}{S(\lambda)^2}\alpha_2 \to \min \tag{2}$$

where $C(\lambda)$ is blood vessel contrast, $S(\lambda)$ spectral sensitivity of the sensor, $\lambda_{max} = 880$ nm wavelength of maximum blood vessel contrast, $\lambda_{min} = 860$ nm wavelength of maximum CCD/CMOS-sensors sensitivity in the IR range, $\alpha_1 = \alpha_2 = 0.5$ weight factors (Pushkareva, 2008). Calculated optimal value of probe wavelength is $\lambda_{opt} = 870 \pm 30$ nm.

Sample images (Figure 7) were acquired by the NIRTI system prototype. The images were registered under the following conditions: probe wavelength $\lambda = 890 \pm 10$ nm, CCD sensor 720x576 pixels, periodontal tissues in vivo.

15
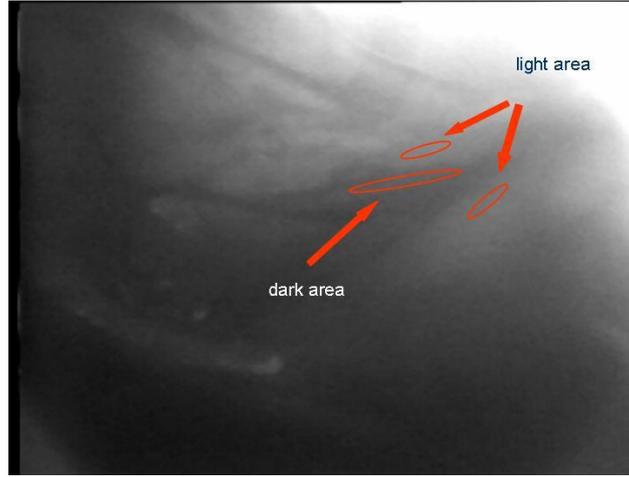
Figure 7. *NIRTI image of periodontal microvasculature.*

The local contrast C_a for each image is given by (3), where $\langle I_w \rangle$ is average intensity of light area pixels and $\langle I_b \rangle$ is average intensity of dark area pixels, i.e. blood vessels (Gonzales & Woods, 2005).

$$C_a = \frac{\langle I_w \rangle - \langle I_b \rangle}{\langle I_w \rangle + \langle I_b \rangle} \tag{3}$$

Assuming that the local image contrast C_a has a normal distribution, the half width of the confidence interval for C_a is $t_\alpha^n S_{C_a}$, where S_{C_a} is root-mean-square error of C_a and t_α^n-Student's coefficient value. A sample capacity $n = 32$ and a significance level $\alpha = 0.05$ provides $t_\alpha^n = 2$. The estimated value of C_a is therefore 0.11±0.14.

3. State of the Art in NIRTI

This chapter gives an overview of some previous studies of NIRTI for caries detection as well as imaging and parameterization of vascular structures.

3.1 NIRTI for early caries detection

Some previous studies have been done on NIRTI for early caries detection. Since the technology is in a relatively early stage, most of the previous research is focused on capturing of images and not the next step, namely image processing. Of course, the image processing is an important part of constructing a system for caries detection and to some extent must be included, but the emphasis in most articles is on the acquisition of images and the optical properties of tissue.

A small survey shows that many of the most relevant studies have been carried out by a research team at University of California. Most of their studies are performed with a NIRTI system working at a wavelength of 1310 nm. The research includes a broad range of investigations concerning topics and phenomena connected to NIRTI, nevertheless, all their studies indicates that NIRTI is a very promising technique for early caries detection. Here follows a summary of some of the most important results of their research. A full description of previous studies can be found in Appendix IV.

Studies on contrast ratio between caries lesions and surrounding enamel depending on sample thickness shows that a contrast ratio of >0.35 is reachable in samples as thick as 6.75 mm (Jones, et al., 2003).

A comparison between a system based on 830 and 1310 nm has also been performed, which is one of the few involving wavelengths in the lower part of the NIR spectrum. Calculation of the contrast ratio between the lesions and surrounding enamel showed that NIRTI at 830 nm provides improved image contrast in the visible range but less image contrast than at 1310 nm (Rechmann, et al., 2004).

Furthermore, studies have been done on detection of the common type of dental decay occurring in the pits and fissures of the occlusal (biting) surfaces, showing that NIRTI imaging provides high contrast between sound and decay areas which easily can be

differentiated from stains, pigmentation and hypomineralization (fluorosis) (Bühler, et al., 2005).

They have described optical properties of dental enamel based on scattering coefficients, scattering phase function, absorption and optical constants. The result shows that demineralization (caries) increases the scattering coefficient with more than two orders of magnitude at 1310 nm. The scattering showed to be mostly forward directed (Darling & Fried, 2005).

The first in vivo study on NIRTI imaging of approximal contact surfaces has also been presented. 33 caries images were acquired from 33 subjects. The lesions were visible on bitewing radiographs but not by clinical examination. All but one of the 33 examined lesions were successfully detected from at least one out of three directions (Staninec, et al., 2010).

Study with the purpose to determine which wavelengths between 1200-1600 nm that provides the highest contrast for caries lesions has been performed. The result shows that NIR wavelengths above 1400 nm have better performance for TI of occlusal caries while 1300 nm is better for proximal surfaces. Further, enamel with lower mobile water content clearly reduced the transparency at all wavelengths (Chung, et al., 2011).

One of the few studies on the topics made outside the University of California has been carried out by Karolinska Institutet in Sweden. Their work was done to characterize a NIRTI system at 1280 and 1400 nm. The results show that features with a size of 250 μm could be detected. The possibility to estimate the position of the lesion by comparing images from two different sides was also investigated (Karlsson, et al., 2010).

3.2 NIRTI of vascular structures

When it comes to the application of NIRTI for imaging of vascular structures the number of previous studies are very limited. However, some research on imaging and quantification of blood vessels from other diagnostic fields has been found. Worth mentioning is that there are a lot of equipment for measuring tissue oxygenation available, even commercially, based on NIR spectroscopy. However, not a single study has been found on NIR transillumination for measuring tissue oxygenation. Here follows a summary of some of the most important

studies made on imaging and quantification of vascular structures. A full description of previous studies can be found in Appendix V.

An automated image processing based technique to determine vascular density has been developed at Massachusetts Institute of Technology. The processing is performed in 3 steps including background correction, thresholding and morphological manipulations (erosion, dilation, skeletonization). Testing of the method on 328 skeletal muscle tissue images showed that analysis time can be decreased from 15 min/image to 30 sec/image (Rieder, et al., 1996).

Another study presents a framework for geometric analysis of vascular structures focusing on quantification of relationships between elements of a vascular network. To test the algorithm it was used to characterize the geometric relationship between cerebral aneurysms and their parent vasculature, all with satisfying results (Piccinelli, et al., 2009).

A method for quantitative analysis of vascular abnormalities has been developed to assist in endovascular treatment planning. The method simplifies the vasculature into a number of parameters which can be used to detect abnormalities. The result shows satisfactory identification of abnormalities and increased repeatability (Wong & Chung, 2006).

A study on background Optical Coherence Tomography (OCT), with 1400 nm NIR light, focusing on micron scale imaging of vascular microstructures has been performed by Hong Kong University of Science and Technology. The study is one of the few involving imaging of blood vessels and presents some examples of structural properties of diagnostic interest (Brezinski, et al., 1996).

Several techniques and methods have been developed for imaging of blood vessel for vascular surgery planning. However, these studies are usually focused on presentation and display of complex 3D-structures and not on quantification and parameterization, which make them less relevant.

4. Problem Statement

This section specifies the problems to be solved by this thesis. The problem is divided into two main parts, one concerning teeth and one involving blood vessel imaging.

The investigation of previous studies (Chapter 3) shows that relatively much research already has been done in the area of NIRTI for caries detection compared to NIRTI for imaging of vascular structures. Taking novelty into count, this thesis will only briefly investigate teeth imaging but instead have its emphasis on developing methods for blood vessel imaging with the goal to automatically quantify vascular structures.

The present research on infrared transillumination is performed on a system with a shorter wavelength than most previous research within the field. The shorter wavelength, 870 nm, permits use of a cheaper kind of IR diode at the expense of lower contrast. Therefore it is interesting, both in the case of teeth and blood vessel images, to develop methods for increasing the contrast level.

4.1 Teeth imaging

As described in chapter 3, this is the traditional use of dental NIRTI. The work in this field is therefore limited to development of methods for contrast enhancement and segmentation of teeth images.

The work includes acquiring reference images (etalon) to use as a basis for development of the algorithms. Images from the present prototype do not provide images with high enough quality, which makes acquiring a reference image even more important at this stage, until the next version of the prototype is developed.

4.1.1 Contrast enhancement

The system's use of the 870 nm wavelength contributes to a new need of contrast enhancement. The first stage of the problem is therefore to develop methods to enhance the contrast of teeth images.

4.1.2 Teeth segmentation

This part of the problem includes development of an algorithm to divide teeth images into different segments of interest. The aim is to develop an algorithm that could be used as a base for further development.

4.2 Blood vessel imaging

Previous research in the area of NIRTI for vascular imaging is very limited and is therefore of great interest. The goal with the processing of blood vessel images is to deliver diagnostically useful output based on information extracted from vascular structures. This includes developing methods for contrast enhancement, segmentation of blood vessels and feature extraction from networks of blood vessels. As with teeth imaging, a set of reference images to develop the algorithms on should be acquired.

4.2.1 Contrast enhancement and segmentation

In order to be able to perform further processing, the first step is to acquire a better contrast between the vascular structures and the underlying tissue. Section 2.3, describing the image formation, evidently shows that the present NIRTI system can provide images with a local contrast value, $C_a \leq 0.25$. To reach sufficient image quality, the desirable value has been estimated to be $C_a > 0.3$ according to previous studies. Except through image processing, the contrast level will also be improved in the next prototype of the system through filtration of radiation backscattered by tissues and reduction of sensor noise level. However, the non image processing related work will not be included in this thesis. The contrast enhancement in turn enables segmentation of blood vessels.

4.2.2 Structural quantification

As mentioned in section 1.2.2, a quantification of vascular structures could allow extraction of structural features which in turn could compose valuable diagnostic information. The first step in this process is to develop a method and a convention for how this quantification should be done. That includes specifying and motivating which parameters that could be interesting to measure and show how these parameters can be used to calculate further properties.

4.2.3 Extraction of structural parameters

Based on the method for quantification, an algorithm should be developed to automatically extract, store and present blood vessel features. Which features to measure, calculate and present should be anchored in diagnostic needs.

5. Results

The aim of this section is to answer the questions and provide solutions to the problems specified in Chapter 4. Cases where the results not completely solve the problem are motivated. All image processing algorithms have been developed in MATLAB 2010b with Image Processing Toolbox.

5.1 Teeth imaging

The first part of the result addresses the problems related to imaging of teeth. This section is divided into three parts where the first one describes how reference images have been acquired, the second involves contrast enhancement and the third presents the methods used for segmentation of the images. As previously mentioned, only a minor part of the work is put into processing of teeth images in favour for blood vessel imaging part.

5.1.1 Teeth images

The current version of the NIRTI system prototype allows capturing of teeth images of the type presented in Figure 8. However, the next version of the prototype, currently under development, will be able to deliver images with higher resolution, contrast level etc. Therefore, and to develop the algorithms to as unbiased images as possible, reference images (etalons) have been acquired. These images consist of thin teeth slices (ca 1 mm) captured with a setup of standard components. That includes a digital IR-camera (VAC-135), an IR-diode (BetLux L513IRBC 880/50nm) and an optical filter (Infinity SCVHMA04FIR) all connected to a PC. See appendix VI-VIII for further details about the equipment. An example teeth slice with some demineralization and color defects is presented in Figure 9.

**Figure 8.** *Teeth image captured by the NIRTI system prototype.*
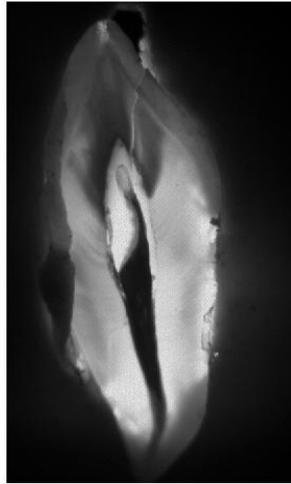
Figure 9. *Sample tooth reference image.*

5.1.2 Contrast enhancement

As a pre-stage before performing further processing, some noise-removing filtering was performed and the image contrast was enhanced to a satisfying level (Figure 10). First of all, a 5x5 Wiener filter is applied to remove the small, but existing, noise in the image. The noise is expected to be higher in the non-reference images and the noise removal procedure will then be of greater importance. Based on the original contrast level (ratio between light and dark areas), a factor indicating how much the contrast should be enhanced is calculated. Finally the contrast is stretched to cover the whole histogram spectrum.
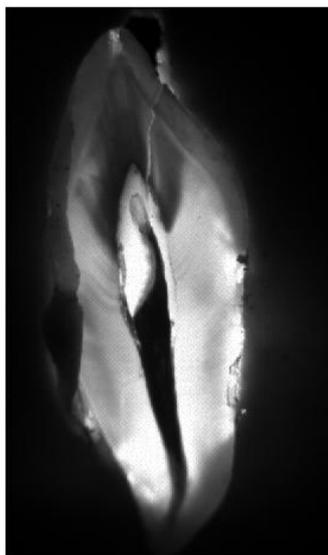

Figure 10. *After filtering and contrast enhancement.*

5.1.3 Segmentation

The next step, in order to identify different parts and areas of the tooth, a local thresholding was performed. The developed method divides the image into small elements whereupon an otsu-method (Otsu, 1979) local thresholding. The number of thresholding layers is optional, the example Figure 11, contains 6 equally distributed layers.
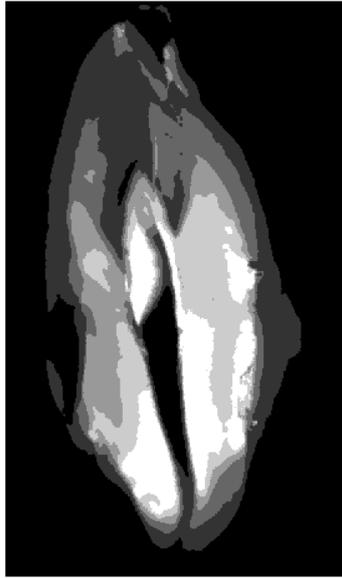
Figure 11. *6 layer "otsu" local thresholding.*

In Figure 12, the 6 thresholding layers are separated and plotted side by side for illustration. These layers can be combined, subtracted etc. to acquired to find teeth irregularities.
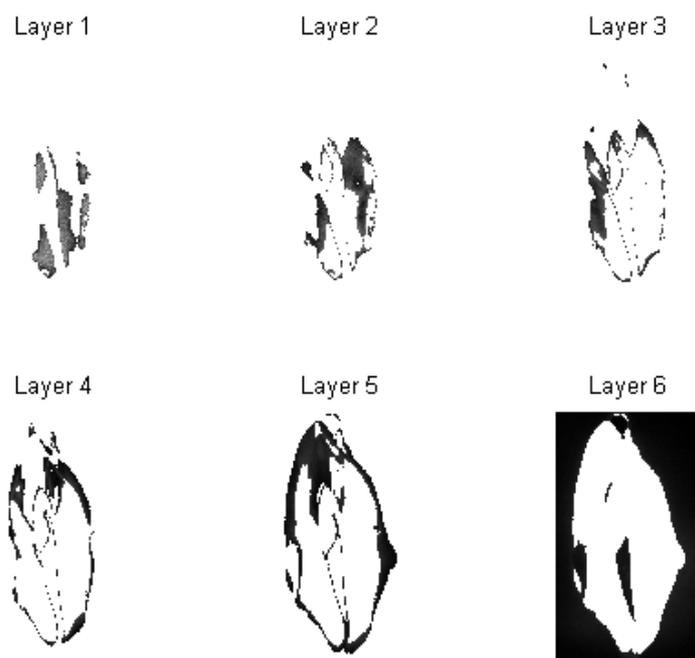
Figure 12. *Thresholding layers 1-6.*

For example, if the layers are combined, more useful masks can be acquired (Figure 13). The number of layers can be adjusted to reach a higher level of separation.
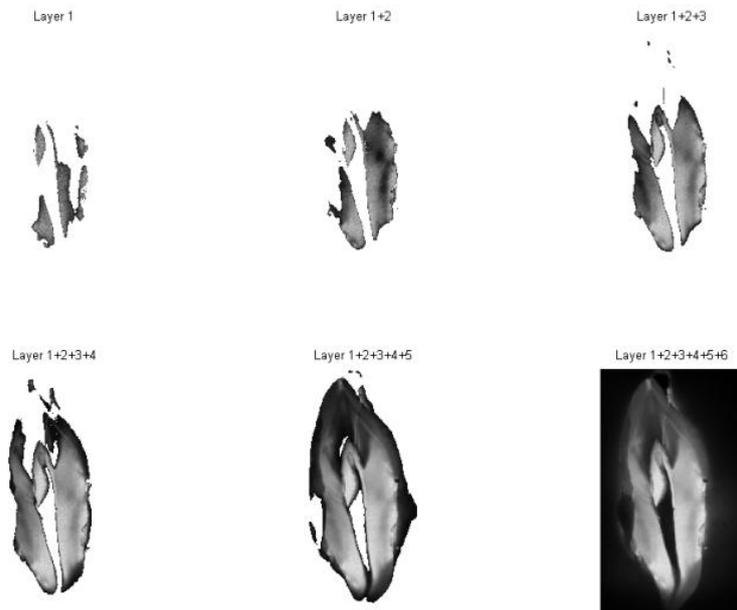


Figure 13. *Thresholding layers combined.*

Based on these layers, different contours of interest can be detected. In Figure 14 and 15, two different contours are plotted on top of the filtered image.
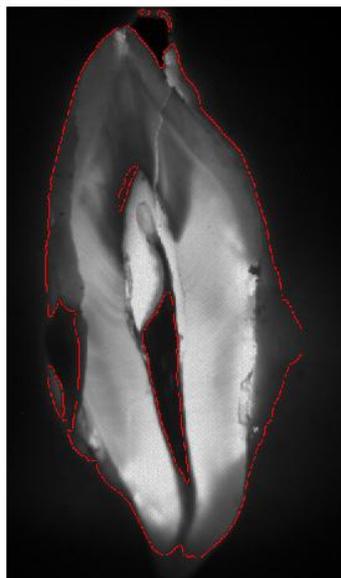
Figure 14. *Tooth outer contour.*
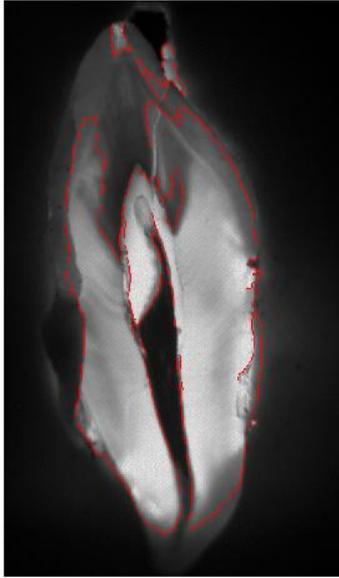
Figure 15. *Tooth inner contour.*

5.2 Analysis of vascular structures

This section presents the results related to blood vessel imaging and analysis of vascular structures.

5.2.1 Blood vessel images

For the development of blood vessel contrast enhancement methods, images from the old version of the system prototype have been used. These images have limited contrast and contain some artifacts (Figure 16). The most severe ones are the light artifacts in the central parts of the image. They come from IR-light which has penetrated straight through the tissue, saturates the detector which gives areas of very high intensity.

Figure 16. *Capture blood vessel image.*

The histogram of the original image (Figure 17) has a very light character and gives very low contrast in the interesting areas, i.e. between vessels and underlying tissue.
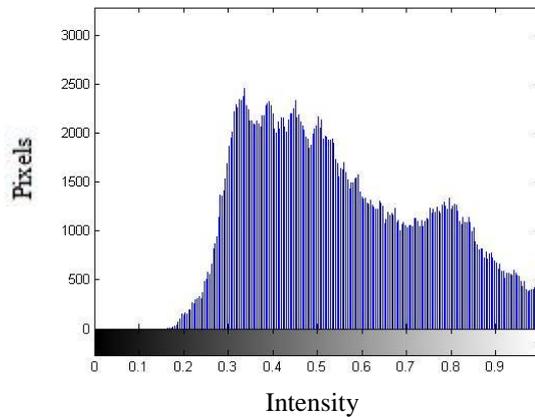
Figure 17. *Histogram corresponding to Figure 16.*

5.2.2 Contrast enhancement and segmentation

The image processing consists of contrast enhancement followed by local thresholding for segmentation and detection of the blood vessels. The first processing step includes stretching the contrast (function *imadjust*) over the whole spectrum (Figure 18 and 19) to maximize the contrast in the interesting parts of the image.
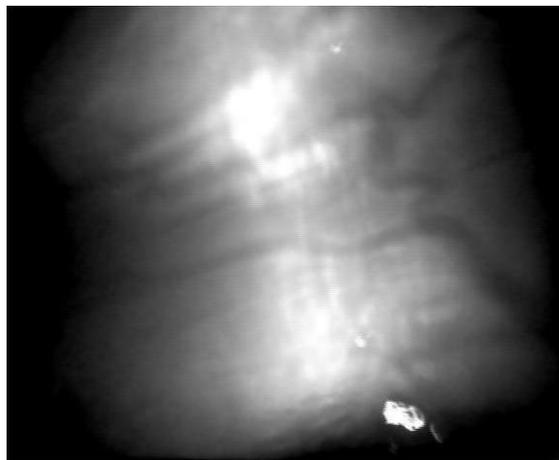
Figure 18. *Stretched histogram and wiener filtering.*

This means that the contrast between the darkest pixels is lost to the benefit of larger contrast in the rest of the image. Already at this stage, the local contrast value calculated with (3) is higher than $C_a > 0.3$.
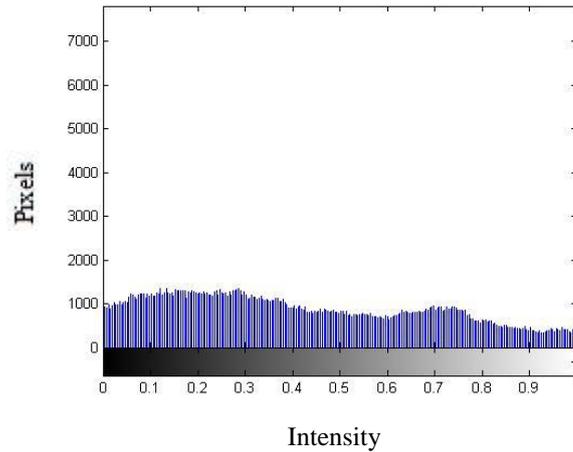
Figure 19. *Histogram corresponding to Figure 18.*

To adopt the histogram even more and rearrange the distribution to wanted configuration, a histogram equalization is then performed (Figure 20). With help of the function *adaptheisteq* with a clip limit of 0.05 and a Rayleigh distribution with alpha 0.37, the histogram is reformatted to have maximum contrast between the blood vessel pixels and the surrounding tissue (Figure 21).
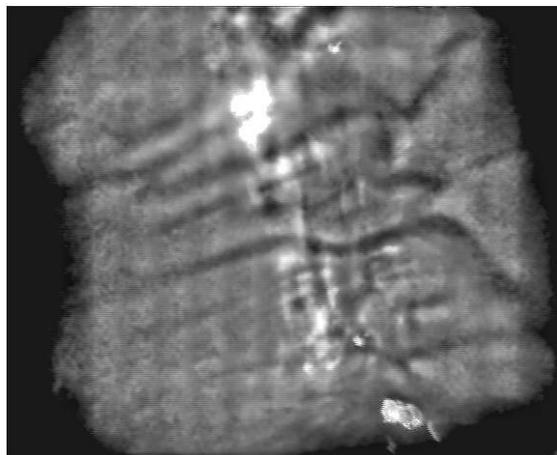
Figure 20. *Histogram equalized image.*

The spike at 0.12 in the histogram is the insipid dark pixels from the previous stage. This method rearranges the histogram to efficiently suppress the light artifacts and globally enhance the blood vessel contrast.

Since the penetration dept of the IR-radiation is a couple of centimeters, different parts of the structure probably are located on different depts. However, in this study, all blood vessel networks are treated as 2D-structures.
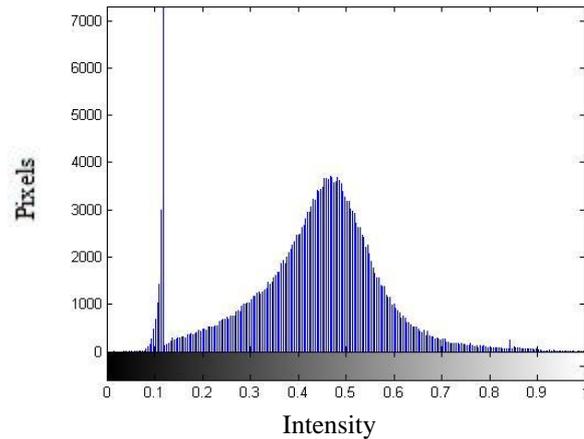
Figure 21. *Histogram corresponding to Figure 20.*

Next step is to detect the blood vessel through local thresholding. Before the thresholding, a median filtering is done to remove some artifacts from the histogram equalized image. Then, an otsu-method (Otsu, 1979) thresholding is performed, including a local thresholding delivering an output with 16 different layers. When investigating the layers, the sum of the first 9 layers shows to form a satisfying blood vessel mask (Figure 22).
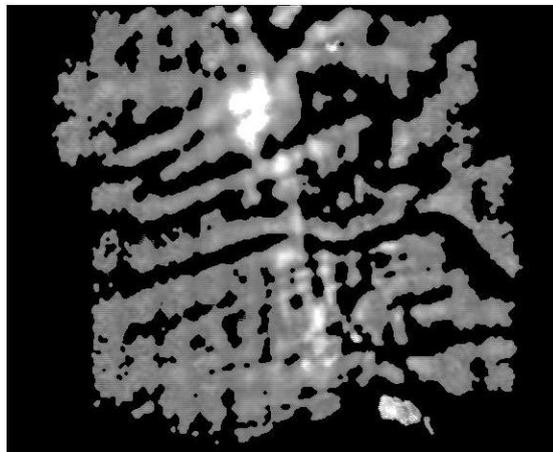
Figure 22. *The sum of the local thresholding layers 1-9.*

The mask is then binarized and small non vascular areas are removed with some morphological manipulations (Figure 23). That includes morphological filling (function *imfill*) to remove white "holes" in the image. This is followed by a morphological closing (function *imclose*) of the image with a 3 pixel disk to widen the vessel areas.

29

Figure 23. *Binarized mask of layers 1-9 after morphological manipulations.*

After that, all objects with a smaller size than 300 pixels are removed (function *bwareaopen*). For illustration, the contour of the mask is detected and plotted on top of the histogram equalized image (Figure 24).
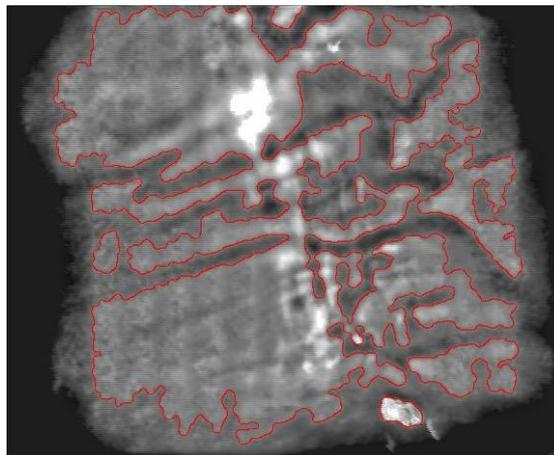
Figure 24. *Contour of mask plotted on top of Figure 20.*

To use as a reference for quality estimation of the algorithm, a mask of areas classified as blood vessels are manually constructed (Figure 25).
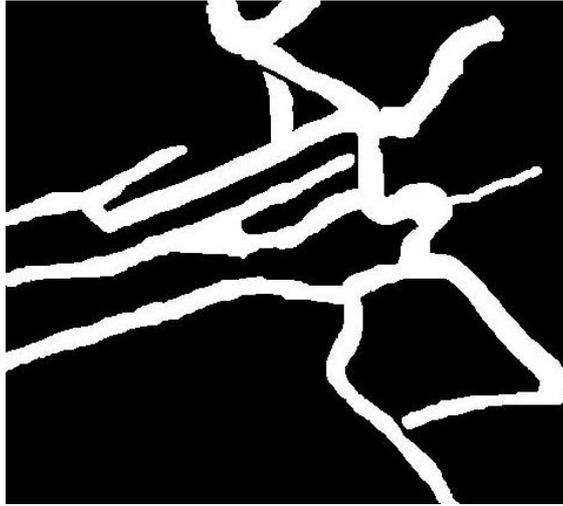
Figure 25. *Manually constructed blood vessel reference mask.*

A comparison between the mask of the detected blood vessels and the reference mask shows that 67 % of the vascular tissue and 93 % of the non vascular tissue is detected correctly. The classification rate is calculated by,

$$Correctly\ detected\ vascular\ tissue = \frac{Number\ of\ vascular\ pixels\ correctly\ classified}{Total\ number\ of\ vascular\ pixels}$$

The rate is naturally calculated similarly for non vascular tissue.

5.2.3 Structural quantification

Structural properties of vascular networks can be divided into dimensional and topological properties (Fleury & Gouyet, 1999). Dimensional properties includes measures as length, diameter and volume and topological properties are referred to as measures on how the vessels are interconnected. The topology describes the vessel interconnection independent of dimensional measures. One way of describing the interconnections, the topological ordering, is the so called generation (or centrifugal) ordering. The vascular tree is here ordered from proximal to distal (Figure 26), where the first branch divides the vessels of the first order into two vessels of the second order and so on (Fleury & Gouyet, 1999).
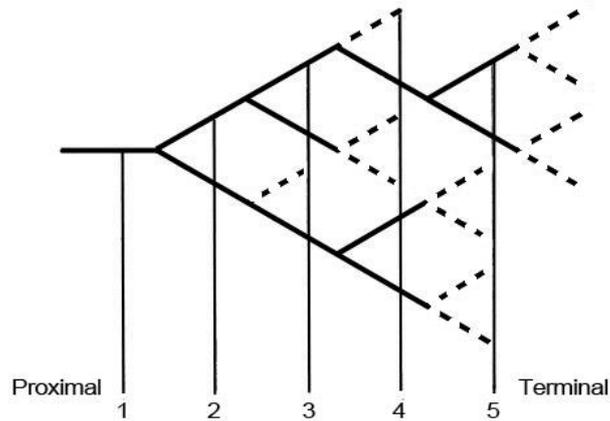
Figure 26. *Generation ordering.*

When diagnosing blood vessel related diseases, vascular density is one of the most interesting properties to examine (Huang, et al., 1996). Vascular density is a function of both vessel length and diameter and describes the volume or space the vascular tree is occupying in the given tissue. Consequently, parameters needed to calculate the vascular density is of high priority when choosing features to measure. Great regard has also been taken to be able to automatically extract the values with image processing methods, i.e. they must be "implementable".

Some conventions and methods for quantification and classification of blood vessel structures for diagnostic purposes already exist (Fleury & Gouyet, 1999), (Huang, et al., 1996), (Davies, 2006). The method developed here is based on a combination of conventional and newly developed parameters. Figure 27 presents a schematic of a vascular structure with parameters of interest marked.
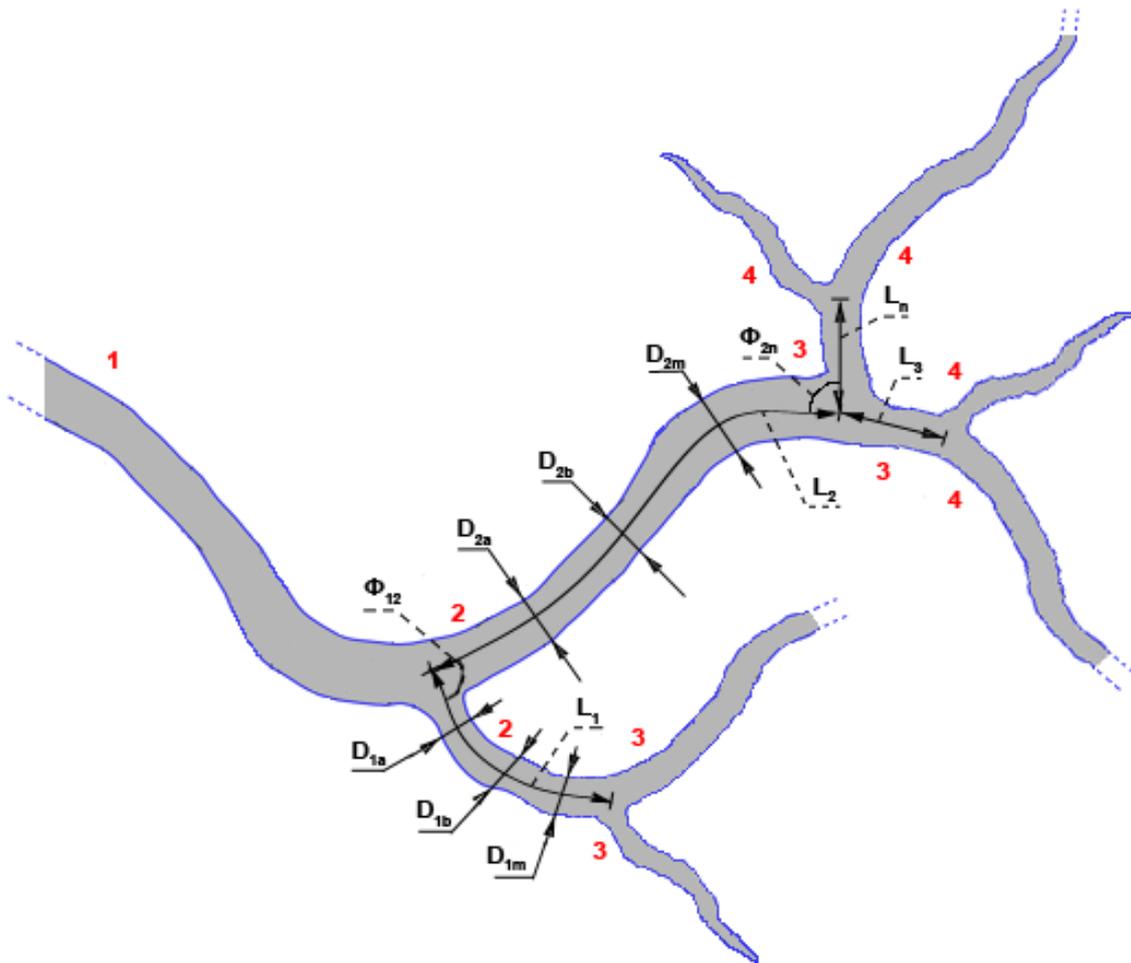
Figure 27. *Vascular structure with parameters of interest.*

The tree structure is built up of blood vessel segments which stretch between an end point and a branching point or between two branching points. The segments, branching points and end points are numbered with increasing numbers starting at 1 depending on the hierarchy level and position. The distance following the vessel central axis between two points enclosing a segment is defined as the vessel length, L_n. The branching angle, Φ_{xy}, is the angle between the two branching segments x and y. The diameter of segment n is measured by averaging a number of diameters, D_{nm}, measured at different places along the segment where m indicates the diameter number. The number of measurement points can be chosen differently depending required precision, size of the vascular network and computational power. Table 1 presents some interesting dimensional and topological parameters.

Table 1. *Dimensional and topological parameters.*

Parameter	Rep.	Comments
Order	1,2,3...k	where k = hierarchic order (red)
Segment	1,2,3...n	where n = segment number
Length	L_n	where n = segment number
Diameter	D_{nm}	where nm = the m:th diameter of segment n
Branching angle	Φ_{xy}	where xy = the point where segment x and y branches
Branching point	1,2,3...b	where b = point number (blue)
End point	1,2,3...e	where e = point number (green)

To present the vascular network characteristics in a more diagnostically useful way, the parameters mentioned above can be used to calculate further properties. In Table 2, a summary of some calculated values of interested are presented.

Table 2. *Calculated vascular structure properties.*

Property	Calculation	Comments
Total length	$L = L_1 + L_2 + L_3 + \cdots + L_n$	The sum of all segment lengths.
Segment mean diameter	$D_n = \frac{D_{na} + D_{nb} + D_{nc} + \cdots + D_{nm}}{m}$	The mean of all diameters of segment n.
Segment area	$A_n = \sum_1^m \frac{L_n \cdot D_{ni}}{m}$	The area of segment n.
Total vascular area	$A_V = A_1 + A_2 + A_3 + \cdots + A_n$	where A_n = area of segment n.

Segment volume	$$V_n = \sum_1^m \frac{L_n \cdot \pi (D_{ni}/2)^2}{m}$$	The volume of segment n assuming that the vessels are cylindrical.
Total vascular volume	$V_V = V_1 + V_2 + V_3 + \cdots + V_n$	where V_n = volume of segment n.
Non vascular tissue area	$A_{non} = A_I - A_V$	where A_I is the total area of tissue.
Vascular density	$D = \dfrac{A_V}{A_I}$	gives vessels/unit area.

5.2.4 Extraction of structural parameters

The purpose of this algorithm is to deliver output values describing the blood vessel structure. The set of rules used by the algorithm in this section is based on the convention for structural quantification presented in the previous section.

As a base for development of the algorithm, a small artificial vascular structure has been designed by hand (Figure 28). The structure is designed with four different hierarchy levels and with different length, diameter and orientation of each segment.
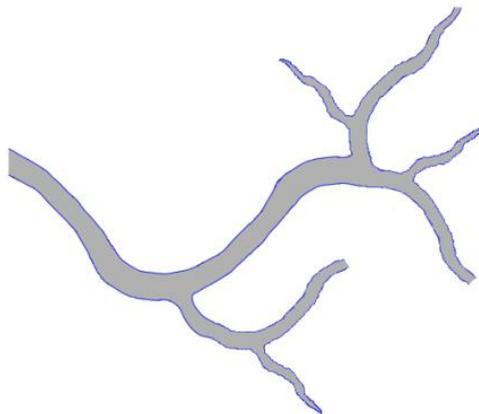
Figure 28. *Sample vascular structure.*

As a first step, the image is binarized and possible irregularities in the vessels are smoothed with the MATLAB function bwmorph(I, 'majority') with the parameter (Figure 29).
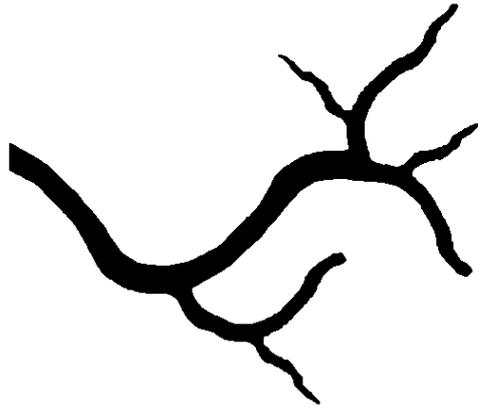
Figure 29. *Binarized vascular structure.*

For use as a reference when calculating the diameter, the contour of the structure is acquired with edge(I, 'prewitt') (Figure 30).
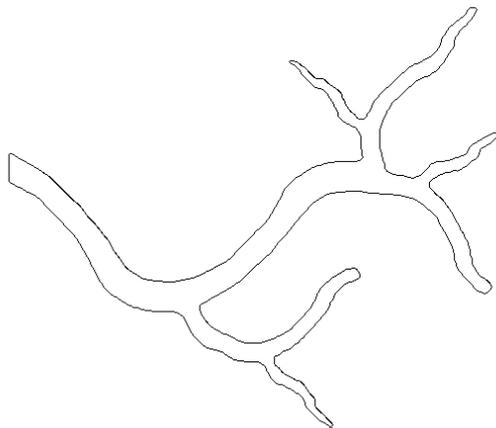
Figure 30. *Contour of the vascular structure.*

The skeleton (the one pixel wide central axis) of the structure is then acquired using bwmorph(I, 'thin', Inf) (Figure 31).
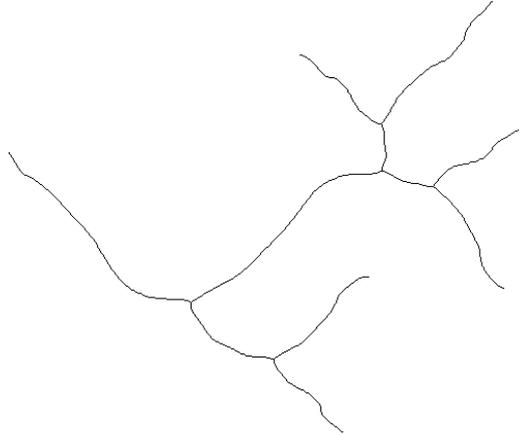
Figure 31. *Skeleton of the structure.*

The end and branching points of the skeleton is detected with the functions bwmorph(I, 'endpoints) and bwmorph(I, 'branchingpoints) respectively (Figure 32).
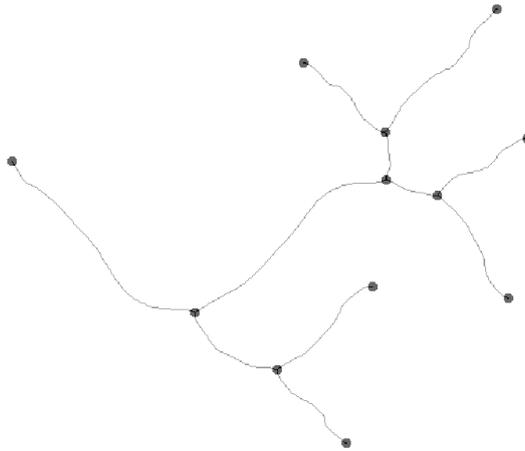
Figure 32. *Skeleton with detected and highlighted branching and end points.*

With the help of these points the elongation of each segment is then determined by looping through all the pixels of the skeleton starting from the very left end point (Figure 33).
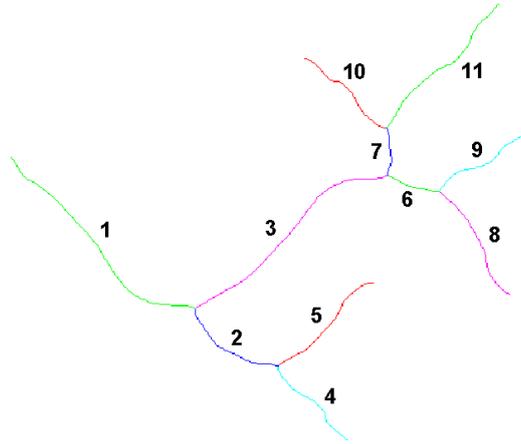
Figure 33. *Detected segments of the structure.*

Number, hierarchy order, length, mean diameter, area and volume are stored for each segment. Segment length is measured as number of pixels between two branching/end points. Diameters are measured as the shortest distance from each skeleton pixel to the contour multiplied by two. Area and volume are then calculated based on these two measures according to Table 2. The result is presented in Table 3.

Table 3. *Measured and calculated segment parameters. The values represent pixel units.*

Segment Number (n)	Hierarchy Order (k_n)	Segment Length (L_n)	Mean Diameter (D_n)	Segment Area (A_n)	Segment Volume (V_n)
1	1	200	29	5786	131395
2	2	93	22	2066	36014
3	2	193	30	5854	139376
4	3	82	13	1049	10535
5	3	101	18	1822	25805
6	3	48	26	1231	24764
7	3	45	24	1061	19653
8	4	103	19	1920	28107
9	4	89	14	1219	13110
10	4	87	12	1061	10149
11	4	132	17	2188	28462
Mean:	3	107	20	2296	42488
Total:	33	1173	223	25256	467370

All values in the table are presented in terms of pixel units and must be translated to a more meaningful unit to be practically useful. The total values of each parameter represent different kinds of dimensional information about the vascular network. The total vascular length,

$$L_V = L_1 + L_2 + L_3 + ... + L_n = 1173 \text{ pixel units}$$

is the total length of the structure skeleton. According to Table 2, the mean diameter of segment n is then calculated through,

$$D_n = \frac{D_{na} + D_{nb} + D_{nc} + \cdots + D_{nm}}{m}$$

where m is the number of measured diameters. In this case one diameter has been measured for each pixel along the segment according to the resolution of the image, 482x567 pixels. The mean diameter can then be used to calculate the area of each segment

$$A_n = \sum_1^m \frac{L_n \cdot D_{ni}}{m}$$

The sum of all segment areas, the total vascular area then becomes,

$$A_V = A_1 + A_2 + A_3 + ... + A_n = 25256 \text{ pixel units}$$

To present the vascular network characteristics in a more diagnostically useful way, the parameters mentioned above can be used calculate further properties. As mentioned previously, one of the most interesting is vascular density i.e. vascular tissue per unit area. Consequently it is calculated as vascular area divided by total area. The total area is,

$$A_I = 482\text{x}567 = 273294 \text{ pixel units}$$

Which gives the vascular density,

$$D_V = \frac{A_V}{A_I} = 0.0924 \, per \, unit \, area$$

This value can in turn be used to get a value of the oxygenation halt of the tissue. Assuming the vessels are cylindrical it is also possible to calculate an expected segment volume,

$$V_n = \sum_1^m \frac{L_n \cdot \pi (D_{ni}/2)^2}{m}$$

and the total expected vascular volume,

$$V_V = V_1 + V_2 + V_3 + ... + V_n = 467370 \text{ pixel units}$$

5.2.5 Test on the captured structure

To test the parameter extraction algorithm, it has been applied to the vascular mask of the captured image in section 5.2.2. Since the quality of the calculated mask is not good enough, the manually constructed mask is used instead (Figure 34). The structure is more complex containing more branches than the one in Figure 28 on which the algorithm was developed.
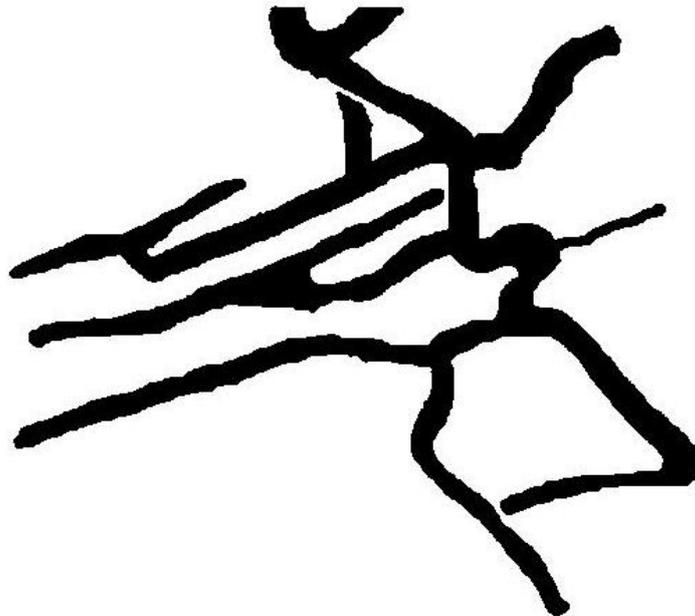

Figure 34. *Inverted version of the vascular mask from section 5.2.2.*

The output from the algorithm is 21 detected segments with length and diameter values, generating a vascular density of 0.1835 per unit area (Figure 35).
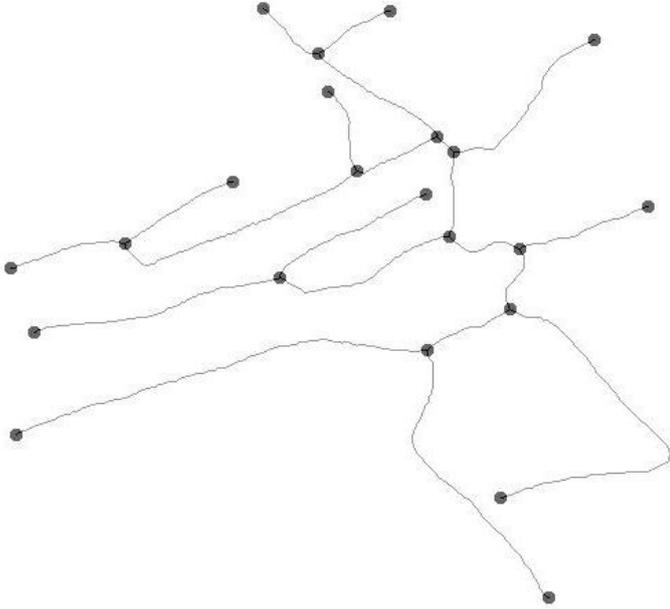
Figure 35, *Skeleton with marked endpoints and branching points.*

6. Conclusions

This is a concluding chapter which includes a comment on the achieved results and a discussion on possible future research.

6.1 Comment on the result

As previously mentioned, the work done regarding caries detection has intentionally been limited. Only some basic algorithms for image enhancement and segmentation have been developed. The local thresholding algorithm can be seen as a first step in development of methods for segmentation of caries lesions. The main reason is mostly because blood vessel imaging early was identified as more novel and interesting, but the work was also partly limited due to lack of teeth samples with early lesions suitable for developing the algorithm further. Images from the currently developed next generation NIRTI system together with better caries affected teeth samples, would ease further development.

The results from the blood vessel imaging are more significant. The comparison between the mask of the detected blood vessels and the reference mask shows that 67 % of the vascular tissue and 93 % of the non vascular tissue is detected correctly. The reason for the low vascular classification rate is mainly the central light artifacts, which is reduced by the algorithm but not completely removed. The easiest way to get rid of the problem would probably be to do better adjustments to the light intensity during the capture. The next generation of the prototype will be able to capture images with better quality and potentially without light artifacts.

Due to the poor quality of the captured images, a simplified blood vessel structure was drawn by hand in order to be able to develop the algorithm without impediment. The chain from captured image to table of extracted parameters can be completed as soon as the captured images hold high enough quality to allow segmentation of the vascular network without artifacts.

Since the quantification algorithm is developed on a specially arranged image, it should just be seen as a platform for further development and proof of concept at this stage. When applying it to a real diagnostic image, some adjustments and corrections are expected to be necessary. However, the algorithm delivered a satisfying result in test made on the vascular mask of the captured image in section 5.2.5.

Using the measured and calculated values presented in Table 3 even more characteristics can be calculated depending of diagnostic application. For example, the relation between different parameters could give valuable information about potential abnormal vascular changes and conditions. Use of the presented method is of course not limited only to infrared transillumination but could also be applied when using other modalities.

The results could in general be summarized as a step towards defining a standard for how to parameterize vascular structures. Further, also development of an algorithm to automatically extract parameters and features from vascular structures. When talking to dentists, the parameter vascular density has shown to be particularly interesting, mostly because it provides a new way to get an indication of blood oxygenation.

6.2 Future Research

In order to develop a NIRTI system able to perform both caries detection and vascular imaging, the system needs to be equipped with at least two different modes, one for each purpose. This is necessary due to the need of different kind of image processing depending on what is imaged. Of course, to include a mode for caries detection, further development of the image processing algorithms must be performed, possibly with inspiration from previous studies in the field (Appendix IV).

To refine the blood vessel segmentation algorithm, an artificial reference object could be constructed and captured without artifacts, similarly to the teeth reference images. In the present state, the algorithm is sensitive to the light intensity conditions. To solve that problem, a normalization of captured image to a defined state could be done, alternatively develop a light intensity independent method, for example wavelet based (Keem & Elbaum, 1997). This would require a more complex algorithm and more computational power.

When choosing parameters to measure, regard has been taken in their relevance for diagnosing conditions mentioned in section 1.2.2, but also interviews with specialist dentists in Sweden. However, based on the information provided by the quantification algorithm including numbers and detected segments, it is of course possible to measure even more and complex parameters. For example information related to orientation of the segments and symmetry.

All blood vessel networks in this study have, for simplicity, been treated as 2D-structures. This leads to some losses in dimensional accuracy and maybe also in division of segments. One important part of future research could therefore be to investigate how much this simplification impacts on the result and in case it is significant, develop a method to compensate for it.

Further development of methods for assisted diagnosis should advantageously be performed in close cooperation with dentists to identify the most valuable information to acquire and present.

Another part of future research involves optimizing the image processing algorithms for real time capturing and presentation. Fast processing is of course a prerequisite for real time diagnosis.

References

Anon., 2012. *Preventive Dentistry.* [Online]
Available at: http://www.affordabledentalcenter.com/dental-services/preventive-dentistry/
[Accessed 10 05 2012].

Belikov, A. et al., 2008. Optimizing the action of laser radiation on soft biological tissues. *Journal of Optical Technology,* 75(1), pp. 8-10.

Brezinski, M. et al., 1996. Optical Coherence Tomography for Optical Biopsy. *Circulation,* 93(6), pp. 1206-1213.

Bühler, C., Ngaotheppitak, P. & Fried, D., 2005. Imaging of occlusal dental caries (decay) with near-IR light at 1310-nm. *Optics Express,* 13(2), pp. 573-582.

Byrnes, J., 2009. *Unexploded Ordnance Detection and Mitigation.* s.l.:Springer.

Chung, S., Fried, D., Staninec, M. & Darling, C., 2011. Multispectral near-IR reflectance and transillumination imaging of teeth. *Biomed Opt Express,* 2(10), p. 2804–2814.

Darling, C. & Fried, D., 2005. Optical properties of natural caries lesions in dental enamel at 1310 nm. *Lasers in Dentistry,* 5687(11), pp. 102-110.

Davies, J., 2006. *Branching morphogenesis.* New York: Springer Science.

Dentists without borders, 2012. [Online]
Available at: http://www.dentistswithoutborders.org
[Accessed 21 May 2012].

Dixit, S., Kim, H., Comstock, C. & Faris, G., 2010. Near infrared transillumination imaging of breast cancer with vasoactive inhalation contrast. *Biomedical Optics Express,* 1(1), pp. 295-309.

Dixit, S., Kim, H., Visser, B. & Faris, G., 2009. Development of a transillumination infrared modality for differential vasoactive optical imaging. *Appl Opt.,* 48(10), pp. 178-186.

Dunn, M. & Conrad, S., 2005. Utilization of Infrared Trans-illumination as an Aid for Peripheral Arterial Access. *Academic Emergency Medicine,* 12(5), pp. 34-35.

Ekestubbe, A., 2012. *University lector, Oral and Maxillofacial Radiology, Sahlgrenska Academy* [Interview] (15 Feb 2012).

Electrophysics, 2012. *A bit of History about Infrared.* [Online]
Available at: http://www.electrophysics.com/View/Viw_TechPrimer_InfraredTutorial.asp
[Accessed 25 Apr 2012].

Fleury, V. & Gouyet, J., 1999. *Branching in Nature: Dynamics and Morphogenesis of Branching Structures, from Cell to River Networks.* Berlin: Springer-Verlag.

Fried, D. et al., 2005. Early caries imaging and monitoring with near-infrared light. *Dental Clinics Of North America,* 49(4), pp. 771-793.

Frydrychowski, A., Rojewski, M. & Guminski, W., 2002. Monitoring of subarachnoid space and cerebrovascular pulsation with near-infrared transillumination/back scattering. *Opto-Electronics Review,* 10(3), pp. 175-183.

Gonzales, R. & Woods, R., 2005. *Digital Image Processing (3rd edition).* s.l.:Prentice Hall.

Gottlow, J., 2012. *Denstist specialized in dental implants* [Interview] (23 Feb 2012).

Hewitt, P., 1993. *Conceptual Physics (2nd ed.).* New York: Addison-Wesley.

Huang, W., Yen, R., McLaurine, M. & Bledso, G., 1996. Morphometry of the human pulmonary vasculature. *J Applied Physiology,* Volume 81, pp. 2123-2133.

Jones, R., Huynh, G., Jones, G. & Fried, D., 2003. Near-infrared transillumination at 1310-nm for the imaging of early dental decay. *Optics Express,* 11(18), pp. 2259-2265.

Karlsson, L. et al., 2010. Near-infrared transillumination of teeth: measurement of a system performance. *J Biomed Opt,* 15(3).

Keem, S. & Elbaum, M., 1997. Wavelet Representations for Monitoring Changes in Teeth Imaged with Digital Imaging Fiber-Optic Transillumination. *IEEE Transactions on medical imaging,* 16(5), pp. 653-663.

Lee, C., Lee, D., Darling, C. & Fried, D., 2010. Nondestructive assessment of the severity of occlusal caries lesions with near-infrared imaging at 1310 nm. *J Biomed Opt,* 15(4).

Mahmood, U. et al., 2012. Near-infrared imaging of the sinuses: preliminary evaluation of a new technology for diagnosing maxillary sinusitis.. *J Biomed Opt,* 15(3).

Matthes, R., 2010. *ilo.org.* [Online]
Available at: http://www.ilo.org/safework_bookshelf/english?content&nd=857170571
[Accessed 29 Apr 2012].

Mohler, E. et al., 2009. Transillumination of the fingers for vascular anomalies: a novel method for evaluating hereditary hemorrhagic telangiectasia. *Genet Med,* 11(5), pp. 356-358.

Otsu, N., 1979. A threshold selection method from gray-level histograms. *IEEE Trans. Sys., Man., Cyber.,* 9(1), pp. 62-66.

Piccinelli, M. et al., 2009. A framework for geometric analysis of vascular structures: application to cerebral aneurysms. *IEEE Trans Med Imaging,* 28(8), pp. 1141-1155.

Pushkareva, A., 2008. *Methods of Mathematical Modeling in Biotissue [in Russian],* St. Petersburg: SpbGU ITMO.

Rechmann, P., Fried, D. & Hennig, T., 2004. Transillumination of interproximal caries lesions with 830-nm light. *Proceedings of SPIE,* 5313(1), pp. 17-22.

Rieder, M., O'Drobinak, D. & Greene, A., 1996. A Computerized Method for Determination of Microvascular Density. *Microvascular Research,* 49(2), p. 180–189.

Schmidt, F., 1999. *Development of a Time-Resolved Optical Tomography System for Neonatal Brain Imaging,* London: Department of Medical Physics and Bioengineering University College London.

Shepro, D., 2006. *Microvascular research.* Boston: Elsevier Academic Press.

Spiridonov, I., 1996. *Laser Treatment and Diagnostic Complex. Codename "Flourite",* Moscow: Department of Biomedical Engineering Systems, BMSTU.

Spiridonov, I., Zharov, V. & Shoshensky, A., 1998. *Способ получения изображения твердых и иягких биотканей (Method for imaging of hard and soft tissues).* Russia, Patent No. 2115927.

Staninec, M., Lee, C., Darling, C. & Fried, D., 2010. In Vivo Near-IR Imaging of Approximal Dental Decay at 1,310 nm. *Lasers Surg Med.,* 42(4), p. 292–298.

Tuchin, V., 2002. *Handbook of Optical Biomedical Diagnostics.* Bellingham, WA: SPIE Press.

Wong, W. & Chung, A., 2006. Augmented Vessels for Quantitative Analysis of Vascular Abnormalities and Endovascular Treatment Planning. *IEEE Transactions on Medical Imaging,* 25(6), pp. 665-684.

Appendices

Appendix I – Published associated articles

Инфракрасная диафаноскопия тканей пародонта

(Infrared transillumination of periodontal tissues)

G. M. Henman, A. A. Taranov, A. V. Kolpakov and I. N. Spiridonov

Journal Meditsinskaya Tekhnika, 2012, No. 4

Модель количественного описания структуры кровеносного русла

(System for quantification of vascular structures)

G. M. Henman, A. A. Taranov, A. V. Kolpakov and I. N. Spiridonov

Students spring conference, Moscow, 19-20 April 2012

Extraction of morphological parameters from vascular structures (published in English)

G. M. Henman, A. A. Taranov, A. V. Kolpakov and I. N. Spiridonov

VIII Russian-Bavarian conference on Biomed. Engineering, St Petersburg, 29-31 May 2012

Методы цифровой обработки изображений для сегментации кровеносного русла

(Image processing methods for segmentation of vascular structures)

G. M. Henman, A. A. Taranov, A. V. Kolpakov and I. N. Spiridonov

Physics and radio electronics in medicine and economics, Souzdal, 27-29 Juni 2012

Appendix II – Alternative diagnostic applications of NIRTI

Application	Description	Maturation
Monitoring of subarachnoid space and cerebrovascular pulsation (Frydrychowski, et al., 2002)	A NIRTI based method for measuring changes in instantaneous width of the subarachnoid space (SAS). This is done to get information on the amplitude of cerebrovascular pulsation in subsequent phases of the cardiac cycle. Studies have been carried out to prove that the pulsation recorded with this technique really has intracranial origin.	Single studies made
Diagnosing maxillary sinusitis (Mahmood, et al., 2012)	Technique for imaging of the maxillary sinuses. The use of NIRTI for this application allows better penetration of structures in deep-tissue compared to visible light. Air-filled and fluid/tissue-filled spaces can be imaged by their differing NIR penetration patterns.	No large scale clinical trials carried out, but studies shows huge potential in the method
Evaluation of hereditary hemorrhagic telangiectasia (Mohler, et al., 2009)	A new NIRTI method for detecting vascular abnormalities in fingers with a handheld illuminator (otoscope). It can be used to detect telangiectases patients with hereditary hemorrhagic telangiectasia.	Single studies made
Imaging of breast cancer (Dixit, et al., 2010), (Dixit, et al., 2009)	A method for imaging breast cancer with NIRTI combined with an inhalation-based contrast. Hyperoxic and hypercarbic gases are inhaled and used as "vasoactive contrast agents" which makes it possible to measure production of changes in endogenous $HbO(2)$ and Hb concentration in blood. The method also provides information about tissue oxygenation, scatter power and differential changes in oxy- and deoxy-	A couple of independent studies and small scale clinical trials

	hemoglobin.	
Aid for Peripheral Arterial Access (Dunn & Conrad, 2005)	Use of NIRTI to improve vascular access by exploting the absorptive qualities of hemoglobin in peripheral vessels. Can be of great help when applying needles to patients where blood vessels are difficult to find.	Widespread method, equipment commercially available

Appendix III – The infrared spectrum

Name	Wavelength	Characteristics
Near-infrared (NIR, IR-A DIN)	750-1400 nm	Except for use in NIRTI it's often used in fiber optic communication cause of its low attenuation losses in the SiO2 glass medium. Also used in image intensifiers like night vision goggles thanks to high light sensitive in this area of the spectrum. The interval is defined by the water absorption properties.
Short-wavelength infrared (SWIR, IR-B DIN)	1400-3000 nm	At 1450 nm, water absorption increases significantly. The range 1530-1560 nm is a spectral region commonly used for long-distance telecommunications.
Mid-wavelength infrared (MWIR, IR-C DIN)	3000-8000 nm	The 3-5 µm range is the atmospheric window in which passive IR "heat seeking" missile are designed to work. The IR signature of the target aircraft is usually the jet engine exhaust plume.
Long-wavelength infrared (LWIR, IR-C DIN)	8–15 µm	This is the region is used for thermal imaging. Based only on thermal emissions, a passive image can be built up without any external light source. Furthermore, this part of the spectrum is used for Forward-looking infrared (FLIR).
Far infrared (FIR)	15 - 1,000 µm	Used for terahertz time-domain spectroscopy, terahertz imaging and fusion plasma physics diagnostics. Can for example be used to detect explosives and chemical warfare agents.

(Byrnes, 2009), (Hewitt, 1993)

Appendix IV – Previous studies on NIRTI for caries detection

Title	Authors	Description
Near-infrared transillumination at 1310-nm for the imaging of early dental decay (Jones, et al., 2003)	*Robert S. Jones, Gigi D. Huynh, Graham C. Jones, Daniel Fried (2003)*	A 1310-nm NIRTI-system used for imaging of slices and whole teeth in order to detect early dental caries (decay). Simulated lesions, which model the optical scattering of natural dental caries, were placed in dental enamel sections. The contrast ratio between the lesions and surrounding enamel was calculated to >0.35 and resolved in samples as thick as 6.75-mm. This study indicates good potential for NIRTI imaging of early dental decay.
Transillumination of interproximal caries lesions with 830 nm light (Rechmann, et al., 2004)	*Rechmann P., Fried D., Hennig T. (2004)*	One of the few studies made on TI in the lower region of the NIR spectrum. Comparison was made between a cheap 830 nm based system with a 1310 nm InGaAs system. Simulated caries lesions, with the same optical properties as natural dental caries, were placed on sound enamel. Calculation of the contrast ratio between the lesions and surrounding enamel showed that NIRTI at 830 nm provides improved image contrast in the visible range but less image contrast than at 1310 nm.
Imaging of occlusal dental caries (decay) with near-IR light at 1310 nm (Bühler, et al., 2005)	*Christopher M. Bühler, Patara Ngaotheppitak, Daniel Fried (2005)*	Detection of the common type of dental decay occurring in the pits and fissures of the occlusal (biting) surfaces. X-ray cannot detect these at an early stage cause of the overlapping topography of the crown of the tooth. 1310-nm NIRTI imaging provides high contrast between sound and decay areas which easily can be differentiated from stains, pigmentation and hypomineralization

		(fluorosis). This study suggest that NIRTI offers many advantages compared to conventional radiographic caries detection methods.
Early caries imaging and monitoring with near-infrared light (Fried, et al., 2005)	*Daniel Fried, John D B Featherstone, Cynthia L Darling, Robert S Jones, Patara Ngaotheppitak, Christopher M Bühler (2005)*	Article discussing development of new optical diagnostic tools for imaging and detection of early dental caries. NIRs optical properties of sound and demineralised (decayed) dental enamel are investigated. A method is described using polarization sensitive optical coherence tomography combined with NIRTI.
Optical properties of natural caries lesions in dental enamel at 1310 nm (Darling & Fried, 2005)	*Cynthia L. Darling, Daniel Fried (2005)*	A description of optical properties of dental enamel based on scattering coefficients, scattering phase function, absorption and optical constants. The study was performed measuring NIR attenuation coupled with Monte Carlo simulations. The result shows that demineralization (caries) increases the scattering coefficient with more than two orders of magnitude at 1310 nm. The scattering showed to be mostly forward directed.
In Vivo Near-IR Imaging of Approximal Dental Decay at 1310 nm (Staninec, et al., 2010)	*Michal Staninec, DDS, PhD, Chulsung Lee, Cynthia L. Darling, PhD, Daniel Fried, PhD (2010)*	Presentation of the the first in vivo study on NIRTI imaging of approximal contact surfaces. 33 caries images were acquired from 33 subjects. The lesions were visible on bitewing radiographs but not by clinical examination. All but one of the 33 examined lesions were successfully detected from at least one out of three directions. Consequently, this study also indicates that NIRTI imaging shows great promise as a non- ionizing screening tool for approximal

		caries lesions.
Nondestructive assessment of the severity of occlusal caries lesions with near-infrared imaging at 1310 nm (Lee, et al., 2010)	*Chulsung Lee, Dustin Lee, Cynthia L. Darling, Daniel Fried (2010)*	Investigation weather lesion contrast can be used to estimate the severity of the lesion. Natural occlusal caries were imaged at 1310 nm with two different NIR imaging technologies (one CMOS-based imaging camera and one InGaAs focal plane array) and classified into 4 categories depending on severity. The result shows that lesion contrast increase significantly with lesion severity for both cameras.
Multispectral near-IR reflectance and transillumination imaging of teeth (Chung, et al., 2011)	*Soojeong Chung, Daniel Fried, Michal Staninec, Cynthia L. Darling (2011)*	Study with the purpose to determine which wavelengths between 1200-1600 nm that provide the highest contrast for caries lesions. Twelve 5-6 mm tooth sections with artificial interproximal lesions and 54 teeth with occlusal lesions were examined. The result shows that NIR wavelengths above 1400 nm have better performance for TI of occlusal caries while 1300 nm is better for proximal surfaces. Further, enamel with lower mobile water content clearly reduced the transparency at all wavelengths.
Near-infrared transillumination of teeth: measurement of a system performance (Karlsson, et al., 2010)	*Karlsson L, Maia AM, Kyotoku BB, Tranaeus S, Gomes AS, Margulis W* (2010)	This work was done to characterize a NIRTI system at 1280 and 1400 nm. Simulated caries lesions attached to tooth sections, consecutively reduced in thickness, were imaged with the NIRTI system. The results show that features with a size of 250 µm could be detected. The possibility to estimate the position of the lesion by comparing images from two different sides was also investigated.

Appendix V – Previous studies on imaging of vascular structures

Title	Authors	Description
A Computerized Method for Determination of Microvascular Density (Rieder, et al., 1996)	*Mark J. Rieder, David M. O'Drobinak, Andrew S. Greene (2002)*	An automated image processing based technique to determine vascular density. The processing is performed in 3 steps including background correction, thresholding and morphological manipulations (erosion, dilation, skeletonization). Testing of the method on 328 skeletal muscle tissue images showed that analysis time can be decreased from 15 min/image to 30 sec/image. The method is also superior in the sense that it is unbiased and nonsubjective.
A Framework for Geometric Analysis of Vascular Structures: Application to Cerebral Aneurysms (Piccinelli, et al., 2009)	*Piccinelli, M. Veneziani, A. Steinman, D.A. Remuzzi, A. Antiga, L. (2009)*	This study presents a framework for geometric analysis of vascular structures focusing on quantification of relationships between elements of a vascular network. The algorithm is based on an open source framework (VMTK) for geometric characterization, image segmentation, mesh generation and computational hemodynamics. To test the algorithm it was used to characterize the geometric relationship between cerebral aneurysms and their parent vasculature.
Augmented Vessels for Quantitative Analysis of Vascular Abnormalities and Endovascular Treatment Planning (Wong & Chung, 2006)	*Wilbur C. K. Wong, Albert C. S. Chun (2006)*	A method for quantitative analysis of vascular abnormalities has been developed to assist in endovascular treatment planning. Starting from a segmented angiography image, the method simplifies the vasculature into a number of parameters which can be used to detect abnormalities. The result shows satisfactory identification of

		abnormalities and increased repeatability.
Optical Coherence Tomography for Optical Biopsy (Brezinski, et al., 1996)	*Mark E. Brezinski, MD, PhD; Guillermo J. Tearney, BA, SM; Brett E. Bouma, PhD; Joseph A. Izatt, PhD; Michael R. Hee, BA, SM; Eric A. Swanson, SM; James F. Southern, MD, PhD; James G. Fujimoto, PhD (1996)*	A study on background Optical Coherence Tomography (OCT), performed with 1400 nm NIR light, focusing on micron scale imaging of vascular microstructures. The study is one of the few involving imaging of blood vessels and presents some examples of structural properties of diagnostic interest.

Appendix VI – Datasheet for IR-diode BetLux-L513IRBC 880/50 nm

T betlux

INFRARED EMITTING DIODES
BL-L513XX-IR

Features:

- 5.0mm Round Type Infrared LED
- High Reliability
- Peak Wavelength at 940, 880, 850nm
- Water Clear, yellow Transparent, Blue Transparent available
- IC compatible /Low current capability.
- Application
- Free air transmission system
- Infrared remote control units with high power requirement
- Smoke detector
- Infrared Camera
- Infrared applied system

RoHs Compliance

ATTENTION OBSERVE PRECAUTIONS ELECTROSTATIC SENSITIVE DEVICES

Electrical-optical characteristics: (Ta=25°C)　(Test Condition: IF=50mA)

Part Number	Chip		Lens Type	$I_{\vec{E}}$	Ir (Vr=5V, uA)	Forward Voltage(VF) Unit:V		Radiant Power (mw/sr)	Viewing Angle 2¦日/2(deg)
	Material	$?_{P^*}$ (nm)				Typ	Max	Typ	
BL-L513IRAC	GaAs	940	Water Clear	50	10	1.40	1.60	30	
BL-L513IRAB	GaAs	940	Blue Trans.	50	10	1.40	1.60	30	
BL-L513IRBC	GaAlAs	880	Water Clear	50	10	1.70	2.00	30	
BL-L513IRBB	GaAlAs	880	Blue Trans.	50	10	1.70	2.00	30	30
BL-L513IRCC	GaAlAs	850	Water Clear	50	10	1.70	2.00	50	
BL-L513IRCB	GaAlAs	850	Blue Trans.	50	10	1.70	2.00	50	
BL-L513IRCY	GaAlAs	850	Yellow Trans.	50	10	1.70	2.00	50	

Absolute maximum ratings (Ta=25°C)

Parameter	Rating	Unit
Forward Current I_F	50	mA
Power Dissipation P_d	150	mW
Reverse Voltage V_R	5	V
Peak Forward Current I_{PF} (Duty 1/10 @1KHZ)	250	mA
Operation Temperature T_{OPR}	-40 to +80	°C
Storage Temperature T_{STG}	-40 to +85	°C
Lead Soldering Temperature TSOL	Max.260±5°C for 3 sec Max. (1.6mm from the base of the epoxy bulb)	°C

* http://www.betlux.com/product/LED_lamp/Super%20Bright%20LED/BL-L513.PDF

Appendix VII – Characteristics for Digital IR-camera VAC-135 USB2.0

| MODEL	VAC-135/VEC-135
Effective pixels	1280 x 1024
CMOS size, inches	1/2" / 1/3"
Horizontal resolutions (*), TV lines	900/800*
Possible images sizes and frame rate for one camera	(SXGA) 1280x1024 - 15 Hz (VGA) 640x480 - 30 Hz (VGA) 640x480 - 60 Hz
Output interfaces	USB 2.0
SNR, dB	50
Sensitivity (F1.2, SNR=20dB)	0,1/ 0,5 Lux
Current consumption , mA	100 (from USB 2.0)
Dimensions, mm	56 x 50 x 92
Temperature range, ^{0}C	+5 … +45
Features	monochrome/ colour

* http://www.evs.ru/eng/doc/List_Mega_A4+.pdf

Appendix VIII – Characteristics for Optical filter Infinity SCVHMA04FIR

SCVHMA-04 FIR
Асферика | ИК-коррекция

Фокусное расстояние	4.0 мм
Формат	1/2"
Фокальное число	F2.0
Управление диафрагмой	фиксированная
Угол обзора	43.1°
Тип крепления	CS

28 мм
20 мм
18 мм
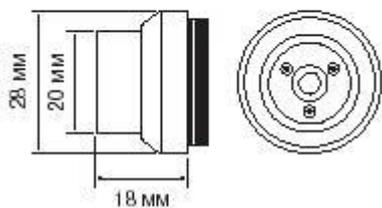
* http://sec-s.ru/infinity_scvhma04fir